mercury attenuator. This irradiator facilitates the irradiation of small animals with dose rate patterns relevant to internal radionuclides, thereby making it possible to investigate the biological effects of time-varying dose rates and to calibrate biological dosimeters.

ACKNOWLEDGMENTS

We thank the Office of Radiation Safety Services at the University of Medicine and Dentistry of New Jersey for the use of their Thomson-Nielson MOSFET dosimeter system. This work was supported in part by U.S. Public Health Service grant CA-54891.

REFERENCES

1. International Commission on Radiological Protection. *Relative biological effectiveness for deterministic effects.* Publication 58. Oxford, England: Pergamon; 1989.
2. International Commission on Radiological Protection. *1990 recommendations.* Publication 60. Oxford, England: Pergamon; 1991.
3. Testa NG, Hendry JH, Lajtha LG. The response of mouse haemopoietic colony formers to acute or continuous gamma irradiation. *Biomedicine* 1973;19:183–186.
4. Wu C-T, Lajtha LG. Haemopoietic stem-cell kinetics during continuous irradiation. *Int J Radiat Biol* 1975;27:41–50.
5. Thames HD, Withers HR, Peters LJ. Tissue repair capacity and repair kinetics deduced from multifractionated or continuous irradiation regimens with incomplete repair. *Br J Cancer* 1984;49(suppl):263–269.
6. Fowler JF. Radiobiological aspects of low dose rates in radioimmunotherapy. *Int J Radiat Oncol Biol Phys* 1990;18:1261–1269.
7. Langmuir VK, Fowler JF, Knox SJ, Wessels BW, Sutherland RM, Wong JYC. Radiobiology of radiolabeled antibody therapy as applied to tumor dosimetry. *Med Phys* 1993;20:601–610.
8. Rao DV, Howell RW. Time dose fractionation in radioimmunotherapy: implications for selecting radionuclides. *J Nucl Med* 1993;34:1801–1810.
9. Howell RW, Goddu SM, Rao DV. Application of the linear-quadratic model to radioimmunotherapy: further support for the advantage of longer-lived radionuclides. *J Nucl Med* 1994;35:1861–1869.
10. Rao DV, Howell RW. On the modeling of the tumor uptake to determine the time-dose-fractionation effect in radioimmunotherapy [Letter]. *J Nucl Med* 1994;35:1562–1564.
11. Hubbell JH. Photon mass attenuation and energy-absorption coefficients from 1 keV to 20 MeV. *Int J Appl Radiat Isot* 1982;33:1269–1290.

Potential and Limitations of Radioimmunodetection and Radioimmunotherapy with Monoclonal Antibodies

Hui Zhu, Laurence T. Baxter and Rakesh K. Jain

Steele Laboratory, Department of Radiation Oncology, Massachusetts General Hospital and Harvard Medical School, Boston; Radiological Science Program, Massachusetts Institute of Technology, Cambridge, Massachusetts

Recently, we developed a physiologically based pharmacokinetic model capable of predicting antibody biodistribution in humans by scaling up from mice. By applying this model to anticarcinoembryonic antigen murine antibody ZCE025, we address several critical issues in radioimmunodetection and radioimmunotherapy, including the optimal antibody doses, the desirable antibody form for cancer detection, the optimal combinations of antibody forms and radionuclides for cancer treatment and the effectiveness of the modality. **Methods:** Under the baseline conditions of a standard 70-kg man with a 20-g tumor embedded in the liver, the model was used to: (a) estimate absorbed doses in tumor and normal tissues, (b) determine dose-dependent antibody uptake in the tumor, (c) simulate tumor-to-background antibody concentration ratio and (d) calculate therapeutic ratios for different antibody forms and radionuclides. Sensitivity analysis further enabled us to determine antibody delivery barriers and to assess the modality under average and favorable tumor physiological conditions. **Results:** By using ZCE025 under the baseline conditions, the model found that Fab was the most suitable form for cancer diagnosis, while ^{131}I combined with F(ab')$_2$ provided the highest tumor-to-bone marrow therapeutic ratio for cancer treatment. Sensitivity analysis showed that antibody permeability was the major barrier for antibody accretion in tumors. It also demonstrated that normal tissue antigen expression at a level lower than in the tumor had little effect on the therapeutic ratio. **Conclusion:** The model demonstrates that: (a) for radioimmunodetection, the most effective antibody form (Fab for ZCE025) was the lower mol weight form, yet not sensitive enough for hepatic metastasis detection; and (b) for radioimmunotherapy, a relatively fast-clearing antibody form (F(ab')$_2$ for ZCE025) in combination with long half-life β^--emitters was optimal, yet inadequate as the sole therapeutic modality for solid tumors.

Key Words: radioimmunodetection; radioimmunotherapy; antibody pharmacokinetics; mathematical modeling; radiation dosimetry

J Nucl Med 1997; 38:731–741

Received Jan. 3, 1996; revision accepted Apr. 10, 1996.

For correspondence or reprints contact: Rakesh K. Jain, PhD, Steele Laboratory, Department of Radiation Oncology, Massachusetts General Hospital, Boston, MA 02114.

Despite limited clinical success, radioimmunodetection (RAID) and radioimmunotherapy (RAIT) remain potentially useful for cancer diagnosis and treatment (*1–3*). Given the technical challenges and complexity, it is essential to optimize treatment variables to fully realize their clinical potential. Our goal in this investigation was to quantitatively address the following critical issues for RAID and RAIT using anticarcinoembryonic antigen (anti-CEA) murine antibody (ZCE025) as an example: (a) Can absorbed doses be estimated a priori from knowledge of physiological and physicochemical parameters using a mathematical model? (b) What is the relationship between antibody dose and antibody uptake in tumors? (c) What are the optimal antibody doses for a high antibody uptake in tumors? (d) Among the three common antibody forms, IgG, F(ab')$_2$ and Fab, which one is the most suitable for cancer detection? (e) What are the optimal combinations of antibody forms and radionuclides that give high therapeutic ratios based on the biodistribution of antibody and physical properties of radionuclides (radiation emissions and half-life)? and (f) How effective are RAID and RAIT under average and favorable tumor physiological conditions?

Resolving these issues requires extensive clinical pharmacokinetic data under well-controlled conditions. Unfortunately, such data are not available for practical reasons. The use of animal models has allowed researchers to individually assess the roles of antibody dose (*4,5*), antibody form (whole immunoglobulin or fragments) (*6–14*), radionuclide (*15,16*) and tumor physiology (*17*) in RAID and RAIT. However, due to the suboptimal conditions used in these studies and experimental variability, the results are not consistent, and the conclusions are subject to interpretation. A prerequisite for optimally using these preclinical data is the ability to scale up the antibody biodistribution from animals to humans and extrapolate the pharmacokinetics to different treatment variables and physiological conditions. To this end, we have recently developed a

physiologically based pharmacokinetic model for antibody biodistribution (*18–20*).

Pioneered by Bischoff and Dedrick (*21*), physiologically based pharmacokinetic modeling uses measurable physiological quantities and anatomically connected organ compartments to quantify drug biodistribution. Compared with other compartmental pharmacokinetic models in which parameters are determined ad hoc by fitting experimental data (*22*), a physiologically based pharmacokinetic model permits a priori predictions, scale up from one mammalian species to another and extrapolation to different conditions (*21,23,24*).

The model we developed can describe the pharmacokinetics of nonspecific (MOPC21) and specific antibodies (anti-CEA murine antibody ZCE025) in nude mice bearing human tumor xenografts (*18*). The model also is capable of predicting their pharmacokinetics in humans with reasonable accuracy by scaling up model parameters from mice (*19*).

In this study, we applied the physiologically based pharmacokinetic model and the MIRD formula to address these critical issues for tumors in the liver and compared the results with studies in the literature. We aimed to evaluate the role of RAID and RAIT using antibody ZCE025 in cancer diagnosis and treatment, especially the management of liver metastases of colorectal cancer, a primary target of anti-CEA antibodies.

MATERIALS AND METHODS

Physiologically Based Pharmacokinetic Model

The mammalian body was modeled as a system of organ compartments connected with the systemic and lymphatic circulation in an anatomic fashion. The compartments included plasma, bone (including bone marrow), heart, lung, liver, kidney, spleen, gastrointestinal tract, skin, muscle and tumor (Fig. 1). The following processes in antibody biodistribution were included in the model: (a) transport through the systemic circulation; (b) extravasation (transcapillary exchange from systemic circulation into the interstitial space); (c) re-absorption from the interstitial space to the systemic circulation through lymphatic circulation; (d) nonspecific binding in the interstitial space; (e) specific binding with tumor-associated antigens; (f) catabolic clearance in tissues; (g) renal clearance; and (h) tumor antigen shedding (Fig. 1). In principle, the model also can include the effect of chemical link and lost label on the observed antibody pharmacokinetics. However, we chose not to include them in this study due to limited experimental information, instead focusing on the physical properties of the radionuclides. We assumed that released labels were rapidly excreted and had little effect on the observed antibody pharmacokinetics.

Sensitivity analysis was performed to determine the relative effect of model parameters on the biodistribution and dosimetry. When considering shed antigens in tumors, we assumed that the free antigens had the same binding kinetics as surface antigens in the interstitial space and were cleared out into the systemic circulation at a constant rate. We also assumed that new antigen was synthesized at the same rate so that the tumor antigen concentration remained constant. For the tumor of small size in the study (20 g), which described micrometastases clinically, the effect of cleared antigens in the systemic circulation on the normal tissue antigen concentrations was neglected in the model. Consequently, a linear whole-body clearance rate for antibody-antigen in tumor was used to quantify the effect of antigen shedding on antibody pharmacokinetics. The details of pharmacokinetic model development are available in the literature (*18,19*). The model equations are given in the Appendix.

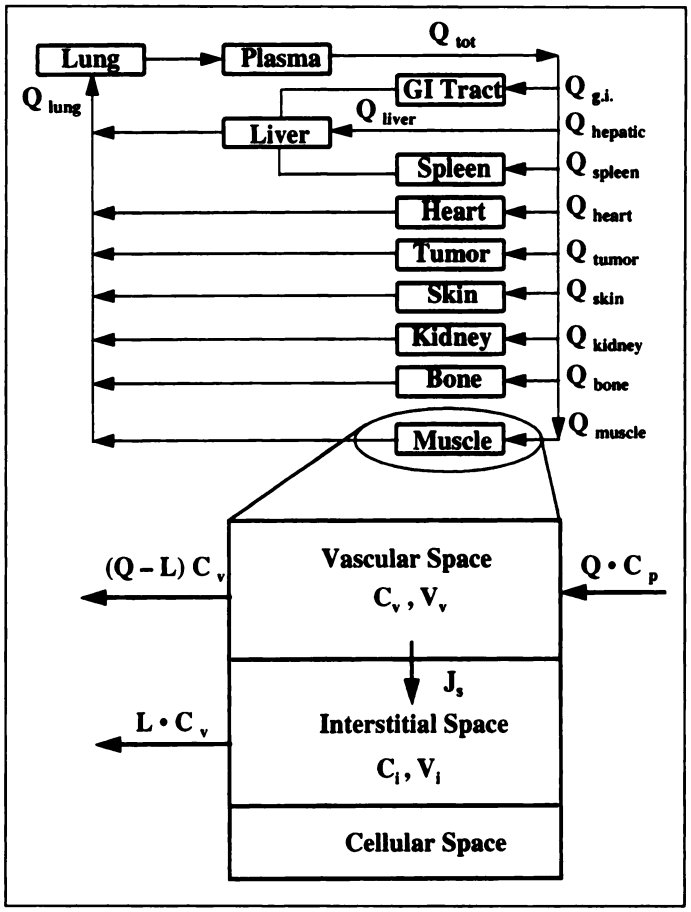

FIGURE 1. Schematic of whole-body compartments for the physiologically based pharmacokinetic model and the subcompartments for tumor. C = antibody concentration in each subcompartment; J_{v-i} = antibody transcapillary exchange; $K^f_{antigen}$ = antibody-specific binding association rate; $K^r_{antigen}$ = antibody-specific binding disassociation rate; L_{organ} = lymphatic flow rate; Q_{organ} = blood flow rate.

Model Parameters and Baseline Conditions

For mice, plasma flow rates, organ volumes, antigen concentration, antibody-antigen binding kinetics, the permeability-surface area products and other antibody-dependent parameters were obtained from the literature. When parameter values were not available in the literature, they were estimated with a weighted nonlinear regression fit to the experimental data for four ^{111}In-labeled antibody species: nonspecific MOPC21 and specific anti-CEA murine antibody ZCE025 IgG, $F(ab')_2$ and Fab fragments (*18*) (Tables 1–3).

For humans, plasma flow rates and organ volumes were obtained from the literature for an average 70-kg standard man (*25*). For the remaining parameters, the murine values were scaled up to humans according to known empirical relations (*19,21*). Vascular and interstitial space volumes, together with fluid recirculation rates were scaled up proportional to body weight. Lymphatic flow rates, permeability-surface products and urine excretion rates were scaled up from mice according to $(\text{body weight})^{3/4}$. Other antibody dependent parameters, such as binding kinetics, pore sizes and reflection coefficients, were kept the same as in mice. The details of parameter estimation are given by Baxter et al. (*19*). The known and estimated parameters formed the baseline conditions in this study (Tables 1–3).

Dose Calculations

The MIRD formula was used to calculate absorbed doses in tumors and normal tissues. Designed for the 70-kg man, this formulation uses standardized anatomy to estimate the internal

TABLE 1
Molecular Species-Dependent Parameters*

Molecular species	R*	B_{max}† M	σ_L‡	σ_S‡	PS_L§ (ml/min/g)		PS_S§ (ml/min/g)		Urine excretion rate (min^{-1})	
					Mouse	Human	Mouse	Human	Mouse	Human
MOPC IgG	1.0	0.00	0.26	0.98	2.66×10^{-6}	3.5×10^{-7}	7.80×10^{-6}	1.0×10^{-6}	0.00033	0.139
ZCE IgG	1.0	1.18×10^{-8}	0.26	0.98	2.66×10^{-6}	3.5×10^{-7}	7.80×10^{-6}	1.0×10^{-6}	0.00026	0.110
ZCE F(ab')$_2$	1.0	1.18×10^{-8}	0.11	0.96	7.98×10^{-6}	1.1×10^{-6}	2.34×10^{-6}	3.1×10^{-7}	0.0011	0.446
ZCE Fab	1.0	2.35×10^{-8}	0.10	0.95	2.42×10^{-5}	3.2×10^{-6}	see Table 3	see Table 3	0.0077	3.262

*See Baxter et al. (*18,19*).
†Antigen concentration from Baxter and Jain (*53*).
‡From Rippe and Haraldsson (*52*).
§Based on albumin data (*52*), scaled by diffusion coefficient in normal tissue. Values for tumor and liver are assumed to be tenfold higher than in other organs.

absorbed doses by assuming a uniform distribution of radioactivity in each organ. A hypothetical 20-g tumor embedded in liver was assumed in the study (i.e., 1800-g liver = 1780-g normal liver tissue and 20-g tumor tissue) (*26,27*). The following equations thus gave the absorbed doses in various tissues:

Tumor:

$$D_{tumor} = \tilde{A}_{tumor}\Delta_{np}/M_{tumor} + (\tilde{A}_{tumor} + \tilde{A}_{n.liver})\Sigma_i\Delta_i\Phi_i(liver \leftarrow liver) + \Sigma_h\tilde{A}_hS(liver \leftarrow h)$$

Liver:

$$D_{liver} = \tilde{A}_{n.liver}\Delta_{np}/M_{n.liver} + (\tilde{A}_{tumor} + \tilde{A}_{n.liver})\Sigma_i\Delta_i\Phi_i(liver \leftarrow liver) + \Sigma_h\tilde{A}_hS(liver \leftarrow h)$$

Others (bone marrow, heart, lung, kidney, spleen, gastrointestinal tract, skin and muscle):

$$D_{organ} = (\tilde{A}_{tumor} + \tilde{A}_{n.liver})S(organ \leftarrow liver) + \Sigma_h\tilde{A}_hS(organ \leftarrow h)$$

Here h includes bone marrow (red marrow), heart, lung, kidney, spleen, gastrointestinal tract, skin and muscle, $\tilde{A}$ is the accumulated activity, Δ_i is the mean energy emitted per nuclear transition for particle i (np for nonpenetrating radiation), Φi (liver → liver) is the specific absorption fraction of energy for target organ liver for particle i emitted in source organ liver, S is the mean dose per unit accumulated activity, M_{tumor} is the liver-embedding tumor tissue mass and $M_{n.liver}$ is the normal liver tissue mass (*25*).

Absorbed Dose Estimation with the Pharmacokinetic Model

To validate the use of the physiologically based pharmacokinetic model in absorbed dose estimation, two different pharmacokinetics (empirical pharmacokinetics by curve fitting and physiologically based model predicted pharmacokinetics) were used to estimate the absorbed dose in humans for ZCE025 IgG. A tri-exponential function $\alpha_1 \exp(-\lambda_1 t) + \alpha_2 \exp(-\lambda_2 t) + (1 - \alpha_1 - \alpha_2) \exp(-\lambda_3 t)$ was fitted to the averaged ^{111}In-labeled antibody ZCE025 IgG pharmacokinetics from 29 patients (body weight 40–100 kg, tumor weight 4–50 g, antibody IgG dose 5–40 mg). The fitted empirical pharmacokinetics were used to calculate the absorbed doses in tumor and critical normal tissues using the MIRD formula. The results were compared with a priori estimates obtained using the physiologically based pharmacokinetic model for ^{67}Cu, ^{90}Y, ^{131}I and ^{188}Re.

TABLE 2
Plasma Flow Rates and Organ Volumes

Organ	Plasma (ml/min)		Total volume (ml)		Vascular volume (ml)		Interstitial volume (ml)	
	Mouse	Human	Mouse‡	Human	Mouse	Human	Mouse	Human
Plasma	4.38*	3000	0.774	2700.0	0.774‡	2700.0	0.000**	0
Bone	0.17*	138	1.500	1500.0	0.080§	150.0	0.280**	279.0
Heart	0.28*	120	0.133	300.0	0.007§	15.0	0.019**	42.9
Kidney	0.80*	630	0.298	284.0	0.030§	28.4	0.101¶	96.6
Liver	1.10*	800	0.951	1809.0	0.095§	180.9	0.190¶	361.8
Lung	4.38*	3000	0.191	999.0	0.019§	99.9	0.057¶	299.7
Muscle	0.80†	413	7.924	35000.0	0.150§	700	1.032¶	4558
Skin	1.21†	220	2.940	6800.0	0.200§	462.0	0.999¶	227
Spleen	0.05†	138	0.100	173.4	0.010§	17.0	0.020¶	34.7
G.I. tract	0.90*	468	3.450	2147.0	0.100§	43.0	0.600†	373.2
Tumor	0.10†	0.564	0.472	20.0	0.033¶	1.4	0.258¶	10.9

*From Gerlowski and Jain (*24*).
†From Baxter et al. (*18*).
‡Determined by averaging the experimental weight data for each organ and assuming a density of 1 g/ml except for bone, 1.5 g/ml. For blood, 55% of volume is assumed to be plasma.
§For well-perfused organs, e.g., kidney, lung, liver, spleen, 10% vascular space is assumed (*54*). For others the vascular space ranges from 2% to 8% of the total volume, and the estimation is based on the experimental data of the plasma and organ at early time points.
¶From Jain (*55*).

TABLE 3
Parameters Fitted for Each Organ*

Organ	J_{iso} ml/min/g		L_{organ} ml/min (ml/min/g)		K^f min^{-1}			PS_s (Fab) ml/min/g	
	Mouse	Human	Mouse	Human	IgG	$F(ab')_2$	Fab	Mouse	Human
Bone	1.4×10^{-5}	1.4×10^{-5}	6.0×10^{-5} (2.7×10^{-5})	2.6×10^{-2}	2.5×10^{-3}	5.5×10^{-4}	3.5×10^{-3}	1.0×10^{-3}	1.3×10^{-4}
Heart	5.6×10^{-5}	5.6×10^{-5}	1.0×10^{-5} (7.5×10^{-5})	4.3×10^{-3}	0.0	3.3×10^{-4}	7.0×10^{-4}	1.0×10^{-4}	1.3×10^{-5}
Kidney	5.6×10^{-4}	5.6×10^{-4}	1.7×10^{-4} (5.7×10^{-4})	7.4×10^{-2}	0.0	1.2×10^{-3}	4.0×10^{-2}	5.5×10^{-3}	7.3×10^{-5}
Liver	4.6×10^{-4}	4.6×10^{-4}	2.0×10^{-4} (2.1×10^{-4})	8.7×10^{-2}	0.0	3.6×10^{-4}	3.3×10^{-3}	1.2×10^{-4}	1.6×10^{-5}
Lung	3.0×10^{-4}	3.0×10^{-4}	1.0×10^{-4} (5.2×10^{-4})	4.3×10^{-2}	0.0	3.0×10^{-5}	2.0×10^{-4}	1.3×10^{-4}	1.7×10^{-5}
Muscle	5.0×10^{-6}	5.0×10^{-6}	6.0×10^{-4} (7.6×10^{-5})	2.6×10^{-1}	0.0	2.4×10^{-4}	5.0×10^{-4}	3.0×10^{-4}	4.0×10^{-5}
Skin	3.0×10^{-5}	3.0×10^{-5}	1.0×10^{-5} (3.4×10^{-5})	4.3×10^{-3}	0.0	7.5×10^{-2}	8.5×10^{-4}	4.7×10^{-4}	6.3×10^{-5}
Spleen	3.0×10^{-5}	3.0×10^{-5}	2.0×10^{-6} (2.0×10^{-5})	8.7×10^{-4}	0.0	6.5×10^{-2}	6.5×10^{-3}	8.5×10^{-4}	1.1×10^{-4}
G.I. tract	1.0×10^{-6}	1.0×10^{-6}	7.0×10^{-4} (2.0×10^{-4})	3.0×10^{-1}	0.0	7.5×10^{-4}	8.5×10^{-4}	9.3×10^{-4}	1.2×10^{-4}
Tumor	1.0×10^{-5}	1.0×10^{-5}	7.0×10^{-5} (1.4×10^{-4})	3.0×10^{-2}	0.80†	0.16*	0.01*	4.5×10^{-4}	6.0×10^{-5}

*MOPC fit J_{iso} and L_{organ}; ZCE-IgG fit only k^f_{bone} and k^f_{tumor}; ZCE-$F(ab')_2$ fit k^f; and ZCE-Fab fit k^f and PS_s. All other parameters kept constant. Lymph flow rates are given on both a per organ and per gram basis (the latter in parentheses).

†Specific binding forward rate constant for tumor, $k^{f,sp}$ min^{-1} ml/pmole; nonspecific k^f taken as zero, with $k^{r,sp} = 0.0085$ min^{-1} and B_{max} for tumor taken as 1.18×10^{-8} M for IgG and $F(ab')_2$, and 2.35×10^{-8} M for the Fab fragment (*53*).

Dose-Dependent Antibody Uptake in Tumor and Optimal Antibody Doses

To determine the relationship between antibody dose and antibody uptake in tumors, the relative antibody uptake in tumors (percent injected dose per gram tissue) was simulated at different antibody doses. The corresponding accumulated activities in tumors were subsequently calculated as a function of antibody dose for IgG, $F(ab')_2$ and Fab in combination with ^{131}I. The optimal antibody doses were selected as doses that achieve 98% or higher of the maximum accumulated activities in tumor.

Radioimmunodetection

Among numerous factors involved in tumor detection, the tumor-to-background antibody concentration ratio is the most critical factor for RAID. The ratio required to successfully identify tumors is a function of tumor size and depth in the body (*28–30*). To determine the feasibility of RAID using anti-CEA antibody ZCE025, the tumor-to-liver antibody concentration ratio as a function of time was simulated under the optimal antibody doses for IgG, $F(ab')_2$ and Fab. This may help discern the optimal antibody forms and the earliest imaging time.

Radioimmunotherapy

The feasibility of RAIT using anti-CEA antibody ZCE025 was assessed by estimating the maximum absorbed doses in tumors achievable with this modality (*31*). In the study, the maximum absorbed dose in tumors was determined as the product of the highest therapeutic ratio and the tolerable absorbed dose for the dose-limiting organ.

Because hematopoietic toxicity is usually the dose-limiting factor in radioimmunotherapy (*32*), tumor-to-bone marrow absorbed dose ratio was calculated as the therapeutic ratio. The hematopoietic toxicity may potentially be circumvented by bone marrow transplantation, and the liver is the foremost site of antibody accretion, tumor-to-liver absorbed dose ratio was thus calculated as an alternative therapeutic ratio. Since the tolerable absorbed doses were usually estimated at 65% of the 50% organ injury doses (4.5 Gy for bone marrow and 20.0 Gy for the liver) (*15,33*), tolerable absorbed doses of 3.0 Gy for bone marrow and 13.0 Gy for liver were estimated.

Sensitivity Analysis

To assess the effect of variability associated with baseline values, the relative sensitivity coefficients of model parameters were calculated as $\Delta R/R$ versus $\Delta P/P$, in other words, the percent change in tumor-to-bone marrow therapeutic ratio R, compared with the percent change in parameter value, P. Positive values for the relative sensitivity mean that the therapeutic ratio increases when the parameter value increases, while negative values mean the opposite, very small absolute values indicate that the therapeutic ratio is insensitive to that parameter.

RESULTS

The success of antibody-guided cancer detection and therapy relies on numerous interacting parameters that may influence the clinical outcome of the modality (*34–36*). With the physiologically based pharmacokinetic model, we optimized the important treatment variables and assessed the effectiveness of RAID and RAIT for anti-CEA antibody ZCE025.

Absorbed Dose Estimation with the Pharmacokinetic Model

The absorbed doses estimated using two different pharmacokinetic methods, empirical pharmacokinetics by curve fitting and physiologically based model predicted pharmacokinetics, are listed in Table 4. The discrepancies between the model prediction and the estimation with curve fitting (typically within 30%) were within the variations associated with the clinical pharmacokinetics. With appropriate adjustable parameters (e.g., tumor permeability) to account for patient variability, the clinical data were more accurately fitted and absorbed doses more precisely estimated (Table 4). The results indicate that the approximate absorbed doses can be estimated from physiological and physicochemical parameters and mouse biodistribution data without unnecessary human studies.

Dose-Dependent Antibody Uptake in Tumors and Optimal Antibody Doses

The accumulated activities in tumors are shown in Figure 2 as a function of antibody dose for ZCE025 IgG, $F(ab')_2$ and Fab in combination with ^{131}I. A nonlinear, saturable relationship was observed for all three antibody forms because of the limited antigen concentration and accessibility in tumors. At low antibody doses, this relationship between antibody dose and antibody uptake in tumors was approximately linear. The relative antibody uptake in tumors (percent injected dose per gram tissue) and the resulting accumulated activity remained largely constant. As the antibody dose increased, a point was reached where oversaturation of tumor antigen sites led to a decrease in the relative antibody uptake in tumors and, consequently, a decrease in the accumulated activity. By contrast, a

TABLE 4
Radiation Doses Estimation with Two Different Pharmacokinetics*

Radionuclide	Absorbed dose (cGy/mCi)								
	Bone	Kidney	Liver	Lung	Muscle	Skin	Spleen	Tumor	G.I.
Estimation by curve fitting									
^{67}Cu	1.30	1.90	3.70	1.80	0.04	0.94	1.40	5.00	1.20
^{131}I	5.20	8.20	18.0	6.50	1.90	2.70	4.60	21.0	5.90
^{188}Re	1.30	2.60	3.70	2.70	0.46	0.95	2.00	4.30	1.20
^{90}Y	5.90	10.0	20.0	10.0	1.60	5.30	7.60	27.0	6.60
Estimation by Physiologically Based Pharmacokinetic Model									
^{67}Cu	1.03	2.33	3.91	1.27	0.04	1.85	1.02	1.40 (4.91)†	0.52
^{131}I	4.11	8.08	15.2	4.08	1.45	7.48	4.93	9.45 (20.82)†	1.98
^{188}Re	1.27	3.19	3.99	1.96	0.30	2.26	1.14	1.06 (4.25)†	0.77
^{90}Y	4.57	13.3	21.1	7.03	1.11	1.11	5.38	5.45 (26.89)†	2.50

*The absorbed doses estimated with two different pharmacokinetics for antibody IgG, i.e., empirical pharmacokinetics by curve fitting, and physiologically based model predicted pharmacokinetics with 10 mg IgG injection dose. A better estimate can be achieved by adjusting appropriate parameters to account for patient variability (see next line).

†The physiologically based model with one adjustable parameter (tumor permeability increased by a factor of 6.5).

linear relationship was observed in the normal tissues under the antigen-free baseline conditions. The relative antibody uptake (percent injected dose per gram tissue) and accumulated activity in the normal tissues thus remained constant (data not shown). On the other hand, saturable dose-dependent uptake is expected and also has been observed clinically in normal tissues expressing minute amounts of antigen (*5*).

Under the baseline conditions, antibody doses lower than 0.093 mmol (14 mg) for IgG, 0.10 mmol (10 mg) for $F(ab')_2$ and 0.50 mmol (25 mg) for Fab achieved 98% or higher of the maximum accumulated activities in tumors and were selected as optimal antibody doses in the study. The observed optimal dose for Fab was lower than that for IgG and $F(ab')_2$ as a result of increased antigen accessibility for the lower mole weight and its faster clearance from the body.

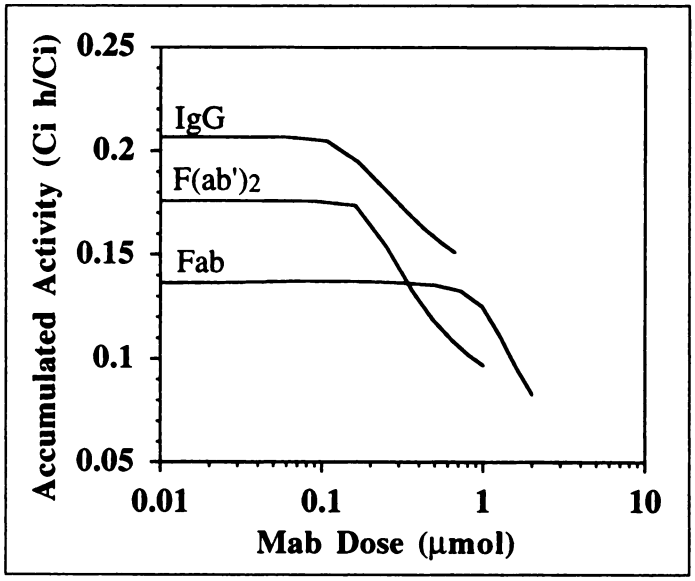

FIGURE 2. Accumulated activity in a tumor as a function of antibody dose for IgG, $F(ab')_2$ and Fab in combination with ^{131}I. The optimal antibody doses were selected to attain 98% or higher of the maximum accumulated activity in tumors. The simulation showed antibody doses lower than 0.093 mmol (14 mg) for IgG, 0.10 mmol (10 mg) for $F(ab')_2$ and 0.50 mmol (25 mg) for Fab were optimal antibody doses under the baseline conditions.

Radioimmunodetection

The tumor-to-liver antibody concentration ratios were simulated and are shown in Figure 3 as a function of time for IgG (14 mg), $F(ab')_2$ (10 mg) and Fab (25 mg). The simulations revealed a lower antibody concentration in tumors than its surrounding liver tissue (i.e., ratio <1.0) during early postinjection period. This implied that a darker tumor may be expected in a brighter background (cold fill-in) under the baseline conditions. As the antibody was excreted from normal tissues, the ratio increased to >1.0 due to antibody-specific binding in tumors. However, this increased tumor-to-liver ratio at a later time postinjection was often beyond the imaging possibility as a result of radioactive decay (*14*). Among different antibody forms, Fab and $F(ab')_2$ fragments gave higher ratios during early periods while IgG gave a higher ratio at later

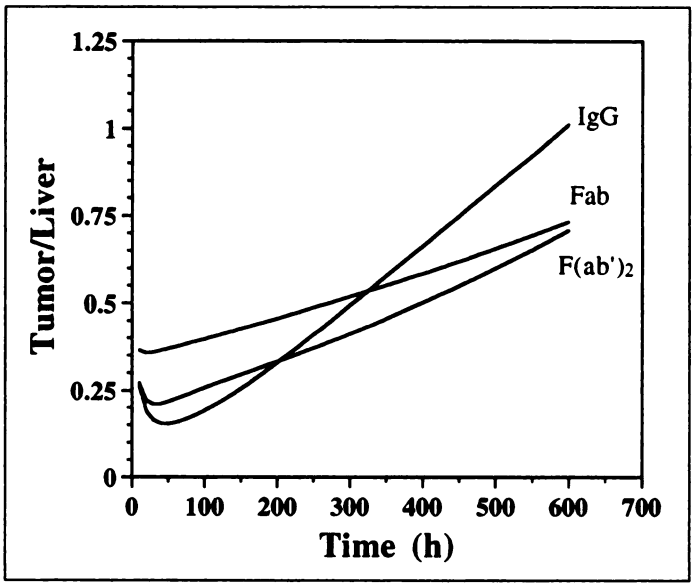

FIGURE 3. The model simulation for antibody IgG, $F(ab')_2$ and Fab tumor-to-liver uptake ratios as a function of time. The simulation indicated a higher tumor-to-liver ratio was attained for Fab than for IgG and $F(ab')_2$ due to its better tumor-penetrating ability.

TABLE 5
Radiation Doses and Therapeutic Ratios

Radionuclide	IgG			$F(ab')_2$			Fab		
	Tumor dose (cGy/mCi)	Tumor/ bone marrow	Tumor/ liver	Tumor dose (cGy/mCi)	Tumor/ bone marrow	Tumor/ liver	Tumor dose (cGy/mCi)	Tumor/ bone marrow	Tumor/ liver
^{67}Cu	1.40	1.36	0.36	1.39	1.45	0.41	1.07	0.78	0.56
^{131}I	9.45	2.30	0.61	8.37	2.64	0.60	6.04	1.44	0.73
^{188}Re	1.06	0.82	0.27	1.15	0.90	0.31	1.00	0.60	0.45
^{90}Y	5.45	1.19	0.26	5.67	1.33	0.30	4.66	0.77	0.46

times, as a result of faster Fab and $F(ab')_2$ penetration into the tumor and slower IgG clearance from the tumor.

Radioimmunotherapy

The absorbed doses in tumor and therapeutic ratios were calculated for different combinations of radionuclides (^{67}Cu, ^{90}Y, ^{131}I and ^{188}Re) and antibody forms (14 mg IgG, 10 mg $F(ab')_2$ and 25 mg Fab). The results are listed in Table 5. Iodine-131 combined with $F(ab')_2$ provided the highest tumor-to-bone marrow absorbed dose ratio of 2.64, and ^{131}I combined with Fab gave the highest tumor-to-liver absorbed dose ratio of 0.73. Accordingly, the maximum absorbed dose of 7.9 Gy in tumors was estimated for ^{131}I combined with $F(ab')_2$ when hematopoietic toxicity was the dose-limiting factor, while a maximum of 9.5 Gy for ^{131}I combined with Fab was estimated when hepatic toxicity was the dose-limiting factor.

Sensitivity Analysis

The relative sensitivity coefficients of the tumor-to-bone marrow therapeutic ratio were calculated for $F(ab')_2$ combined with ^{90}Y and ^{131}I. The results are shown in Figure 4. The results showed that tumor vascular permeability, tumor fluid recirculation rate and tumor fluid drainage were the most sensitive parameters, while moderate changes in tumor plasma flow rate and antibody-antigen affinity have a minimal effect on the therapeutic ratio.

The calculation also demonstrated that an antigen expression in bone marrow at 10% of the tumor level resulted in only a 1.7% increase in absorbed dose in bone marrow for short-lived ^{90}Y and 2.8% for long-lived ^{131}I, which had minimal effect on the therapeutic ratios. The sensitivity analysis found that tumor antigen shedding resulted in a decrease in tumor absorbed dose of 7.3% for ^{131}I and 5.3% for ^{90}Y at a low whole-body antibody-antigen clearance rate of 5 days, 22.8% for ^{131}I and 20.6% for ^{90}Y at a moderate rate of 1 day, and 37.8% for ^{131}I and 49.6% for ^{90}Y at a high rate of 5 hr.

DISCUSSION

The physiologically based pharmacokinetic model offers an idealized but unified framework to explore the parameter space through sensitivity analysis and is thus applicable to antibodies with different physical and biochemical properties, including binding affinity and targeted antigen density.

Dose-Dependent Antibody Uptake in Tumors and Optimal Antibody Doses

It is important to note that while the model determined the optimal antibody doses under well-defined tumor physiological conditions, the doses may not be applicable to situations with different tumor physiological conditions and antibody properties. Since subsaturating antibody doses were shown to give high relative antibody uptake in tumors, low antibody doses with high labeling specificity were recommended.

Important Parameters and Antibody Delivery Barriers

Sensitivity analysis indicated that the antibody extravasation is the major determinant of antibody accretion in tumors. Consequently, increasing antibody permeability would give the highest payoff in radioimmunodetection and therapy (*35–37*). Notably, the tumor plasma flow rate was not a sensitive parameter. This conclusion, however, was based on the hypothetical well-perfused tumor in the model. In the heterogeneous tumor vasculature, increasing blood flow rate and/or making perfusion more uniform may change the distribution pattern, such as open new pathways. This would increase the tumor vascular permeability-surface area product, which would improve the delivery of antibodies to tumor.

The sensitivity analysis demonstrated that normal tissue (e.g., bone marrow) antigen expression at a lower level than in tumor had little effect on the therapeutic ratio. This result, in agreement with certain clinical observations (*38*), was surprising

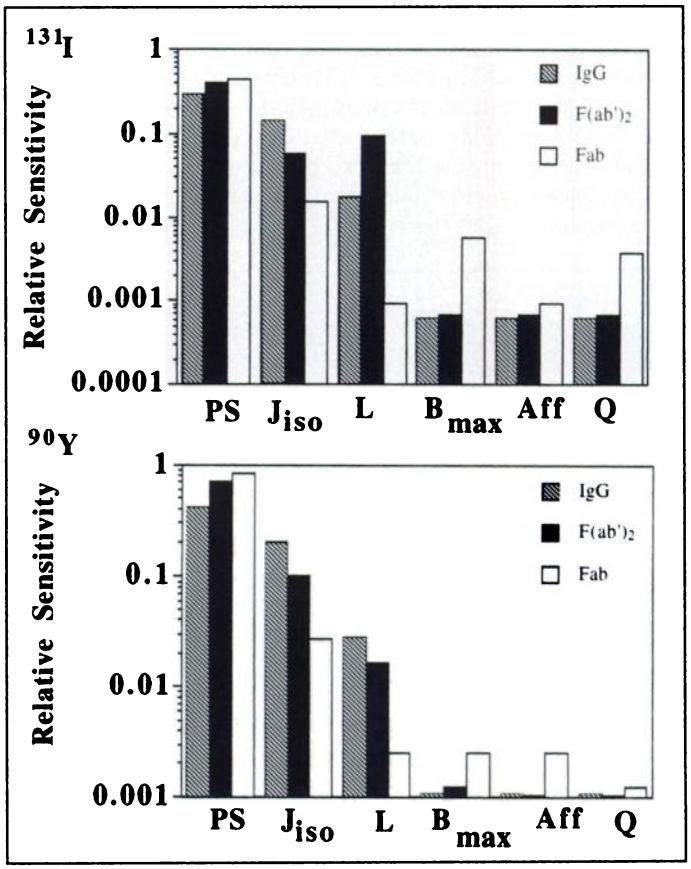

FIGURE 4. The sensitivity analysis for ^{90}Y and ^{131}I, in combination with antibody IgG, $F(ab')_2$ and Fab, for important model parameters: tumor plasma flow rate Q, tumor fluid drainage rate L, tumor fluid recirculation rate J_{iso}, tumor vascular permeability PS (both large and small pores), tumor antigen express B_{max}, antibody-antigen binding affinity Aff.

TABLE 6
Comparison of Antibody Carriers

Study		Injection dose (μg)	Plasma half-life (hr)	Tumor uptake %id/g (48 hr)	T/B (4–12 hr)	T/B (48–72 hr)
Wahl et al. (*56*)	IgG	10–20	T_β = 50.4	2.6	T/B = 0.7, T/L = 2.8	T/B = 1.9, T/L = 7.8
Mouse (CEA)	F(ab')$_2$	10–20	T_β = 30.0	1.1	T/B = 1.3, T/L = 5.2	T/B = 2.4, T/L = 6.2
	Fab	10–20	T_β = 20.2	0.1	T/B = 0.8, T/L = 2.8	T/B = 1.5, T/L = 2.4
Harwood et al. (*9*)	IgG	6	T_β = 36.6	3.0	N/A	T/B = 3.7, T/L = 2.0
Mouse (CEA)	F(ab')$_2$	8	T_β = 6.9	0.5	T/B = 1.5, T/L = 2.58	T/B = 26, T/L = 37
Colapinto et al. (*57*)	IgG	5	T_α = 7.9, T_β = 31.0	16.5	T/B = 2.0	T/B = 4.7, T/L = 21.1
Mouse (glioma Ag)	F(ab')$_2$	3.3	T_α = 4.4, T_β = 17.7	4.2	T/B = 4.7	T/B = 60.5, T/L = 20.3
Endo et al. (*7*)	IgG	10	T_β = 33	5.80	N/A	T/B = 0.88, T/L = 3.65
Mouse (lung cancer Ag)	F(ab')$_2$	10	T_β = 16	1.12	T/B = 0.57, T/L = 1.47	T/B = 1.17, T/L = 2.87
	Fab	10	T_β = 9	0.14	T/B = 1.13, T/L = 3.96	T/B = 1.00, T/L = 1.00
Pedley et al. (*13*)	IgG	50	T_β = 69.5	16.4	T/B = 0.4	T/B = 2.2, T/L = 21.1
Mouse (CEA)	F(ab')$_2$	100	T_β = 32.3	4.2	T/B = 1.0	T/B = 34.0, T/L = 20.3
Buchegger et al. (*58*)	IgG	60	T_β = 80.6	25.0	T/B = 0.9, T/L = 2.25	T/B = 3.5, T/L = 10
Mouse (CEA)	F(ab')$_2$	110	T_β = 9.2	7.0	T/B = 1.9, T/L = 8.3	T/B = 20, T/L = 30
Hendrix et al. (*10*)	IgG	0.5–5	T_β = 62.4; 72.2; 106.6	3.0	T/B = 0.3	T/B = 0.5
Mouse (PLAP, CEA)	F(ab')$_2$	2.5–25	T_β = 4.3; 5.4	1.0	T/B = 1.0	T/B = 7.5
Gerresten et al. (*8*)	IgG	25	T_β = 61.3	11.9	N/A	T/B = 3.3, T/L = 16.0
Mouse (22 kD Ag)	F(ab')$_2$	28	T_β = 33.7	4.4	N/A	T/B = 7.3, T/L = 24.7
Milenic et al. (*11*)	IgG	2.5	T_α = 0.65, T_β = 113	18	T/B = 0.3, T/L = 0.8	T/B = 4.1, T/L = 3.6
Mouse (TAG 72)	F(ab')$_2$	5	T_α = 0.43, T_β = 12	13.9	T/B = 3.7, T/L = 3.4	T/B = 82.9, T/L = 8.4
	Fab	10	T_α = 0.15, T_β = 1.5	2.7	T/B = 7.8, T/L = 2.7	T/B = 144.2, T/L = 19.1
	sFv	12	T_α = 0.06, T_β = 1.5	0.7	T/B = 1.4, T/L = 2.2	T/B = 30.2, T/L = 16.1
van Dijk et al. (*6*)	IgG	5	T_β = 22.8	13.5	T/B = 1.3, T/L = 2.0	T/B = 7.9, T/L = 3.8
Mouse (carcinoma Ag)	F(ab')$_2$	5	T_β = 7.9	5.1	T/B = 2.7, T/L = 5.7	T/B = 42.5, T/L = 36.4

given the present attention on normal tissue antigen expression. On the other hand, tumor antigen shedding, which reduces antibody residence time and thus absorbed dose in tumors, was found to have an important effect on RAIT at a moderate and/or high clearance rate.

The antibody-antigen binding affinity, proportional to the target-to-background ratio under idealized conditions (*39*), was also found to have a limited effect on the therapeutic ratios. This suggests that increasing antibody-antigen affinity beyond the baseline level (10^{11} M^{-1}) to improve target-to-background ratio would be limited by physiological barriers.

Limitations and Potential of Radioimmunodetection

The most suitable antibody form for cancer detection would be the one that achieves the highest tumor-to-background ratio 24–48 hr after injection. Yet the studies to date are not conclusive mainly because of the suboptimal treatment variables (Table 6). Under the baseline conditions, the model indicates that antibody form with a lower mole weight was generally better in achieving high tumor-to-background ratios. In agreement with the majority of experimental studies, Fab was found to be a better choice than IgG and F(ab')$_2$ for RAID using antibody ZCE025.

Even with Fab, RAID gave low tumor-to-background signal ratios. For a gamma-ray camera using subtraction method, a ratio of approximately 2.5 is required for the hypothetical 20-g tumor (i.e., 1.7-cm diameter) at 5 cm depth (*30*). This suggests that hepatic metastasis detection is unlikely under the baseline conditions. Since the hepatic metastasis is among the most common for colorectal cancer, the role of RAID using ZCE025 in cancer diagnosis may be limited (*1*).

Tumor physiology is known to be highly variable and depends strongly on tumor type and size. Sensitivity analysis indicated that in patients with increased tumor vascular permeability (sixfold higher than the baseline value), four times increased tumor-to-background signal ratio can be achieved (Fig. 3). This would permit the detection of such a tumor in the first two days after the antibody administration. This not only reaffirmed the need for patient identification for suitable physiological conditions (e.g., proper tumor types and stages) (*40*) but also suggested the key parameters and criteria in such a screening.

Limitations and Potential of Radioimmunotherapy

Dosimetric calculations indicate that radionuclides with long half-lives, such as ^{131}I, resulted in higher therapeutic ratios because of the specific antibody binding in tumor. Radionuclides with localized radiation, such as ^{90}Y, also gave rise to high therapeutic ratios. Long half-life and localized radiation emission (compared to tumor size) are the desirable features to achieve high therapeutic ratios.

For the majority of carcinomas of aerodigestive tract (lung, stomach, liver and gastrointestinal), the 60%–70% tumor control dose is about 35 Gy with external beam irradiation (*41*). However, the maximum absorbed dose in tumors was 9.5 Gy under the baseline conditions and 28.5 Gy under favorable tumor conditions with six times higher tumor permeability. Though the radiobiological criterion derived from external

TABLE 7
Comparison of Different Pharmacokinetic Analyses

	Pharmacokinetic model	Tumor	Optimal MAb doses	Optimal MAb carrier	Desirable radionuclides for RAIT	Optimal MAb-Ag affinity
Empirical pharmacokinetics	Wessels et al. (*15*)	500-g solid liver tumor in 70-kg patient	N/A	N/A	^{186}Re and ^{90}Y	N/A
	Yorke et al. (*16*)	20-g/500-g solid liver tumor in 70-kg patient	N/A	$F(ab')_2$	^{186}Re, ^{90}Y and ^{135}Sm	N/A
Compartment pharmacokinetics	Eger et al. (*42*)	N/A	IgG: 3.5 mg	N/A	N/A	N/A
	Thomas et al. (*43*)	10-ml tumor with 100 times higher [Ag] than normal tissues	IgG: 1.5 mg	10^{-3} s^{-1} clearance rate	N/A	10^{11}–10^{12} M^{-1}
	Sung et al. (*44*)	10-n*M* antigen concentration	0.45 mg for low affinity, 130 mg for high affinity	N/A	N/A	10^{9} M^{-1}
	Baxter et al. (*19*)	20-g solid liver tumor in 70-kg patient	IgG: 15 mg $F(ab')_2$: 14 mg Fab: 20 mg	$F(ab')_2$	^{131}I and ^{90}Y	10^{11} M^{-1}
Distributed pharmacokinetics	Weinstein et al. (*45–49*)	10 m*M*	N/A	Fab	N/A	10^{7}–10^{8} M^{-1}
Clinical observations	Goldenberg et al. (*1*)	N/A	IgG: 0.25 mg, up to 10–40 mg	MAb fragments	N/A	N/A

beam irradiation may not be fully applicable to RAIT, the calculations suggest that RAIT using ZCE025 as the sole therapeutic modality for solid tumor was inadequate. In addition to patient identification, other antigen targets and strategies, such as tumor vascular targeting and multistep strategies, are needed or combination therapies must be applied (*35–37*).

Comparison with Previous Studies

To evaluate the physiologically based pharmacokinetic model, we compared our major conclusions with previously published studies. The results are summarized in Table 7.

Based on human empirical pharmacokinetics, Wessels et al. (*15*) were among the first to determine proper radionuclides for RAIT. Yorke et al. (*16*) further tried to optimize antibody-radionuclide combination based on extrapolated human pharmacokinetics from murine data through direct volume scaling. These studies have investigated a wide variety of radionuclides and reached a similar conclusion to that of this study. Limited by the empirical nature, these studies did not address other critical issues, and the extrapolation by assuming identical volume normalized antibody pharmacokinetics may not be reliable.

Eger et al. (*42*), Thomas et al. (*43*) and Sung et al. (*44*), using ad hoc compartmental models, along with Baxter et al. (*19*), using a physiologically based pharmacokinetic model, have addressed several critical issues in RAID and RAIT. The studies have demonstrated a dose-dependent antibody uptake in tumors with the desirable IgG dose varying from 1.5 mg (*43*) to 130 mg (*44*) due to the different physiological conditions. The applicable analyses (*16,19,45–49*) also have indicated that $F(ab')_2$ and Fab are better choices than IgG in cancer diagnosis. All studies have indicated that increasing antibody-antigen affinity beyond a certain limit would little improve the antibody tumor uptake (*19,42–44*). The discrepancies in optimal affinity among these studies were mainly due to the estimated antigen accessibility, a function of tumor vascular permeability and antigen concentration. A similar conclusion on binding affinity also has been implied using distributed models due to binding-barrier (*45–49*).

Overall, the present model is in agreement with other theoretical analyses with certain quantitative discrepancies because of the different baseline conditions. The strength of the present model lies in its ability to address these issues in an integrated way and use measurable physiological parameters for greater reliability.

Model Limitations

The model analysis was based on the pharmacokinetics of the murine antibody ZCE025 in a standard patient under average tumor physiological conditions. It did not fully address the variability associated with tumors and the effect of modulations nor did it include the effect of a chemical link and the fate of lost labels, alternative antigen targets and antibody constructs. In particular, there are certain limitations with the model assumptions and special cautions must be taken to interpret the results.

In the model, we assumed a hypothetical tumor with fixed tumor size and antigen concentration. The simulations were, therefore, the averaged effects without considering tumor growth or regression during treatment and heterogeneity among different tumors.

Another assumption is the uniform antibody distribution within tissue, a feature of lumped pharmacokinetic models. Though a good approximation for low mole weight agents, the distribution is known to be heterogeneous for macromolecules (*50*). Moreover, under significantly elevated vascular permeability, the antibody distribution may be limited by its diffusion in the extracellular matrix. Distributed models and microdosimetric methods must be developed to evaluate such effects. Nevertheless, for β-emitting radionuclides with a range of a few millimeters and tumors with limited size, the assumption is reasonable under the time scale of interest, especially for micrometastases, the primary targets of RAID and RAIT.

CONCLUSION

Under the baseline conditions for a 20-g liver cancer in a standard 70-kg man using anti-CEA murine antibody ZCE025, the physiologically based pharmacokinetic model suggested that Fab was the most suitable antibody form for cancer diagnosis, while ^{131}I combined with $F(ab')_2$ provided the highest tumor-to-bone marrow therapeutic ratio for cancer treatment. Sensitivity analysis showed that antibody permeability was the major barrier for higher antibody accretion in tumor. The analysis also demonstrated that normal tissue antigen expression at a lower level than in tumor had little effect on the therapeutic ratio. The model demonstrated that smaller antibody forms are better choices for cancer diagnosis, while radioimmunotherapy requires relatively fast-cleaning antibodies, such as $F(ab')_2$, with long half-life β^--emitters. Most importantly, the analysis suggested that RAID and RAIT with monoclonal antibody alone may have a limited role in cancer management. Therefore, it is necessary to develop new antigen targets and strategies and to identify the subgroup of patients that is most likely to benefit from these modalities in clinical settings.

APPENDIX A: NOMENCLATURE

B_{max}	Tumor-associated antigen concentration (M)
C_{pl}	Antibody plasma concentration (M)
$C_{v,organ}$	Antibody concentration in the vascular space (M)
$C^f_{i,organ}$	Free antibody concentration in the interstitial space (M)
$C^b_{i,antigen}$	Antibody-antibody concentration in the interstitial space (M)
$C^b_{i,organ}$	Bound antibody concentration in the interstitial space (M)
$C_{t,organ}$	Antibody average concentration (M)
$J_{iso,organ}$	Fluid recirculation flow rate (= flow rate through large pore into the interstitial space for L = 0) (ml/min)
$J_{S,organ}$, $J_{L,organ}$	Transcapillary fluid flow rate (from the vascular space to the interstitial space) (ml/min) through small and large pores
$J_{v\text{-}i,organ}$	Transcapillary solute exchange rate (moles/min)
$k_{EL,antigen}$	Antibody-antigen clearance rate via shedded free antigen (min^{-1})
$k_{EL,organ}$	Bound antibody clearance rate due to catabolism and degradation (min^{-1})
k^f, k^r	Association and disassociation rate constants for nonspecific binding between antibody and extracellular matrix (min^{-1})
$k^{f,sp}$, $k^{r,sp}$	Association (M^{-1} min^{-1}) and disassociation (min^{-1}) rate constants for specific binding between antibody and antigen
L_{organ}	Lymph flow rate (ml/min)
$Pe_{L,organ}$, $Pe_{S,organ}$	Peclet number, ratio of convection to diffusion across large and small pores ($Pe = J(1 - \sigma)/PS$)
$PS_{L,organ}$, $PS_{L,organ}$	Permeability-surface area product (min^{-1}) for large and small pores
Q_{organ}	Plasma flow rate (ml/min)
$R_{organ,x}$	Partition coefficient of antibody between the vascular and interstitial spaces
U	Excretion rate constant through urine clearance in the kidney (ml/min)
$V_{i,organ}$	Volume of interstitial space (ml)
$V_{v,organ}$	Volume of vascular space (ml)
$V_{t,organ}$	Volume of total organ (ml)
$\sigma_{L,x}$, $\sigma_{S,x}$	Osmotic reflection coefficient of antibody for large and small pores

APPENDIX B: MATHEMATICAL MODEL AND GOVERNING MASS BALANCE EQUATIONS

The mass balance equations describe the transport of antibodies throughout the body with each organ divided into two subcompartments, the vascular space and extravascular space (Fig. 1). The equations were solved using LSODE with Gear's method for stiff equations (*51*). Between the vascular space and extravascular space, the net flux of antibodies across the capillary between plasma and interstitial fluid is determined by the two-pore model proposed by Rippe (*52*):

$$\begin{aligned} J_{v\text{-}i,organ} &= J_{L,organ}(1 - \sigma_{L,x})C_{v,organ} + PS_{L,organ}(C_{v,organ} \\ &\quad - C^f_{i,organ}/R_{organ,x}) \frac{Pe_{L,organ}}{e^{Pe}_{L,organ} - 1} + J_{S,organ} \\ &\quad \cdot (1 - \sigma_{S,x})C_{v,organ} + PS_{S,organ}(C_{v,organ} \\ &\quad - C^f_{i,organ}/R_{organ,x}) \frac{Pe_{S,organ}}{e^{Pe}_{S,organ} - 1} \text{ and } J_{L,organ} \\ &= J_{iso,organ} + \alpha_L L_{organ}; \; J_{S,organ} \\ &= - J_{iso,organ} + \alpha_S L_{organ}. \end{aligned}$$

Mass Balance Equation for Plasma

$$\begin{aligned} V_{pl}(dC_{pl}/dt) &= (Q_{lung} - L_{lung})C_{v,lung} + L_{lung}C^f_{i,lung} + L_{liver}C^f_{i,liver} \\ &\quad + L_{gi}C^f_{i,gi} + L_{spleen}C^f_{i,spleen} + L_{kidney}C^f_{i,kidney} \\ &\quad + L_{tumor}C^f_{i,tumor} + L_{skin}C^f_{i,skin} + L_{muscle}C^f_{i,muscle} \\ &\quad + L_{bone}C^f_{i,bone} + L_{heart}C^f_{i,heart} - (Q_{liver} + L_{gi} + L_{spleen} \\ &\quad + Q_{kidney} + Q_{tumor} + Q_{skin} + Q_{muscle} + Q_{bone} \\ &\quad + Q_{heart})C_{pl}. \end{aligned}$$

There is an additional constraint on the volumetric flow rates:

$$\begin{aligned} Q_{lung} &= Q_{liver} - L_{liver} + Q_{kidney} - L_{kidney} + Q_{tumor} - L_{tumor} \\ &\quad + Q_{skin} - L_{skin} + Q_{muscle} - L_{muscle} + Q_{bone} - L_{bone} \\ &\quad + Q_{heart} - L_{heart}. \end{aligned}$$

Mass Balance Equations for Lung

Vascular space:

$$\begin{aligned} V_{v,lung}(dC_{v,lung}/dt) &= (Q_{liver} - L_{liver})C_{v,liver} + (Q_{kidney} \\ &\quad - L_{kidney})C_{v,kidney} + (Q_{tumor} \\ &\quad - L_{tumor})C_{v,tumor} + (Q_{skin} - L_{skin})C_{v,skin} \\ &\quad + (Q_{muscle} - L_{muscle})C_{v,muscle} + (Q_{bone} \\ &\quad - L_{bone})C_{v,bone} + (Q_{heart} - L_{heart})C_{v,heart} \\ &\quad - (Q_{lung} - L_{lung})C_{v,lung} - J_{v-i,lung}. \end{aligned}$$

Interstitial space:

$$\begin{aligned} V_{i,lung}(dC^f_{i,lung}/dt) &= J_{v-i,lung} - k^f_{lung}C^f_{i,lung}V_{i,lung} \\ &\quad + k^r_{lung}C^b_{i,lung}V_{i,lung} - L_{lung}C^f_{i,lung} \\ V_{i,lung}(dC^b_{i,lung}/dt) &= k^f_{lung}C^f_{i,lung}V_{i,lung} - k^r_{lung}C^b_{i,lung}V_{i,lung} \\ &\quad - k_{EL,lung}C^b_{i,lung}V_{i,lung}. \end{aligned}$$

Mass Balance Equations for Liver

Vascular space:

$$V_{v,liver}(dC_{v,liver}/dt) = (Q_{gi} - L_{gi})C_{v,gi} + (Q_{spleen} - L_{spleen})C_{v,spleen} + (Q_{liver} - Q_{gi} - Q_{spleen} + L_{gi} + L_{spleen})C_{pl} - (Q_{liver} - L_{liver})C_{v,liver} - J_{v-i,liver}.$$

Interstitial space:

$$V_{i,liver}(dC^{f}_{i,liver}/dt) = J_{v-i,liver} - k^{f}_{liver}C^{f}_{i,liver}V_{i,liver} + k^{r}_{liver}C^{b}_{i,liver}V_{i,liver} - L_{liver}C^{f}_{i,liver}$$

$$V_{i,liver}(dC^{b}_{i,liver}/dt) = k^{f}_{liver}C^{f}_{i,liver}V_{i,liver} - k^{r}_{liver}C^{b}_{i,liver}V_{i,liver} - k_{EL,liver}C^{b}_{i,liver}V_{i,liver}.$$

Mass Balance Equations for Tumor

Vascular space:

$$V_{v,tumor}(dC_{v,tumor}/dt) = Q_{tumor}C_{pl} - (Q_{tumor} - L_{tumor})C_{v,tumor} - J_{v-i,tumor}.$$

Interstitial space:

$$V_{i,tumor}(dC^{f}_{i,tumor}/dt) = J_{v-i,tumor} - k^{f,sp}_{antigen}C^{f}_{i,tumor}(B_{max} - C^{b}_{i,antigen})V_{i,tumor} + k^{r}_{antigen}C^{b}_{i,tumor}V_{i,tumor} - k^{f,sp}_{tumor}C^{f}_{i,tumor}V_{i,tumor} + k^{r}_{tumor}C^{b}_{i,tumor}V_{i,tumor} - L_{tumor}C^{f}_{i,tumor}$$

$$V_{i,tumor}(dC^{b}_{i,antigen}/dt) = k^{f,sp}_{antigen}C^{f}_{i,tumor}(B_{max} - C^{b}_{i,antigen})V_{i,tumor} - k^{r,sp}_{antigen}C^{b}_{i,antigen}V_{i,tumor} - k_{EL,antigen}C^{b}_{i,antigen}V_{i,tumor}$$

$$V_{i,tumor}(dC^{b}_{i,tumor}/dt) = k^{f}_{tumor}C^{f}_{i,tumor}V_{i,tumor} - k^{r}_{tumor}C^{b}_{i,tumor}V_{i,tumor} - k_{EL,tumor}C^{b}_{i,tumor}V_{i,tumor}.$$

Mass Balance Equations for Kidney

Vascular space:

$$V_{v,kidney}(dC_{v,kidney}/dt) = Q_{kidney}C_{pl} - (Q_{kidney} - L_{kidney})C_{v,liver} - UC_{v,kidney} - J_{v-i,kidney}.$$

Interstitial space:

$$V_{i,kidney}(dC^{f}_{i,kidney}/dt) = J_{v-i,kidney} - k^{f}_{kidney}C^{f}_{i,kidney}V_{i,kidney} + k^{r}_{kidney}C^{b}_{i,kidney}V_{i,kidney} - L_{kidney}C^{f}_{i,kidney}$$

$$V_{i,kidney}(dC^{b}_{i,kidney}/dt) = k^{f}_{kidney}C^{f}_{i,kidney}V_{i,kidney} - k^{r}_{kidney}C^{b}_{i,kidney}V_{i,kidney} - k_{EL,kidney}C^{b}_{i,kidney}V_{i,kidney}.$$

Mass Balance Equations for Other Organs

Vascular space:

$$V_{v,organ}(dC_{v,organ}/dt) = Q_{organ}C_{pl} - (Q_{organ} - L_{organ})C_{v,organ} - J_{v-i,organ}.$$

Interstitial space:

$$V_{i,organ}(dC^{f}_{i,organ}/dt) = J_{v-i,organ} - k^{f}_{organ}C^{f}_{i,organ}V_{i,organ} + k^{r}_{organ}C^{f}_{i,organ}V_{i,organ} - L_{organ}C^{f}_{i,organ}$$

$$V_{i,organ}(dC^{b}_{i,organ}/dt) = k^{f}_{organ}C^{f}_{i,organ}V_{i,organ} - k^{r}_{organ}C^{b}_{i,organ}V_{i,organ} - k_{EL,organ}C^{b}_{i,organ}V_{i,organ}.$$

In each organ, the average antibody concentration is the weighted average of the concentration within each subcompartment:

$$C_{t,organ} = (C_{v,organ}V_{v,organ} + C^{f}_{i,organ}V_{i,organ} + C^{b}_{i,organ}V_{i,organ})/V_{t,organ}.$$

ACKNOWLEDGMENT

This work was supported by National Cancer Institute grant R35-CA-56591.

REFERENCES

1. Goldenberg D, Larson S. Radioimmunodetection in cancer identification. *J Nucl Med* 1992;33:803–814.
2. Goldenberg DM. Introduction to the fifth conference on radioimmunodetection and radioimmunotherapy of cancer. *Cancer Res* 1995;55:5708s–5709s.
3. Larson SM. Improving the balance between treatment and diagnosis: a role for radioimmunodetection. *Cancer Res* 1995;55:5756s–5758s.
4. Rogers GT, Harwood RB, Pedley RB, Boden J, Bagshawe KD. Dose-dependent localization and potential for therapy of $F(ab')_2$ fragments against CEA studied in a human tumor xenograft model. *Br J Cancer* 1986;54:341–344.
5. Halpern S, Hagan P. Effect of protein mass on the pharmacokinetics of murine monoclonal antibodies. *J Nucl Med* 1985;26:818–819.
6. van Dijk J, Zegveld ST, Fleuren GJ, Warnaar SO. Localization of monoclonal antibody G250 and bispecific monoclonal antibody CD3; G250 in human renal-cell carcinoma xenografts: relative effects of size and affinity. *Int J Cancer* 1991;48:738–743.
7. Endo K, Kamma H, Ogata T. Radiolabeled monoclonal antibody 15 and its fragments for localization and imaging of xenografts of human lung cancer. *J Natl Cancer Inst* 1988;80:835–842.
8. Gerrestsen M, Quak JJ, Suh JS, et al. Superior localization and imaging of radiolabeled monoclonal antibody E48 $F(ab')_2$ fragment in xenografts of human squamous cell carcinoma of the head and neck and of the vulva as compared to monoclonal antibody E48 IgG. *Br J Cancer* 1991;63:37–44.
9. Harwood PJ, Boden J, Pedley RB, Rawlins G, Gogers GT, Bagshawe KD. Comparative tumor localization of antibody fragments and intact IgG in nude mice bearing a CEA-producing human colon tumor xenograft. *Eur J Cancer Clin Oncol* 1985;21:1515–1522.
10. Hendrix PG, Dauwe SE, van de Voorde A, Nouwen EJ, Hoylaerts MF, de Broe ME. Radiolocalization and imaging of stably HPLAP-transfected MO4 tumors with monoclonal antibodies and fragments. *Br J Cancer* 1991;64:1060–1068.
11. Milenic DE, Yokota T, Filpular DR, et al. Construction; binding properties; metabolism; and tumor targeting of a single-chain Fv derived from the pancarcinoma monoclonal antibody CC49. *Cancer Res* 1991;51:6363–6371.
12. Nieroda CA, Milenic DE, Carrasquillo JA, Schlom J, Greiner JW. Improved tumor radioimmunodetection using a single-chain Fv and g-interferon: potential clinical applications for radioimmunoguided surgery and g scanning. *Cancer Res* 1995;55:2858–2865.
13. Pedley RB, Boden JA, Boden R, Dale R, Begent RHJ. Comparative radioimmunotherapy using intact or $F(ab')_2$ fragments of ^{131}I anti-CEA antibody in a colonic xenograft model. *Br J Cancer* 1993;68:69–73.
14. Behr T, Becker W, Hannappel E, Goldenberg DM, Wolf F. Targeting of liver metastases of colorectal cancer with IgG; $F(ab')_2$ and Fab' anti-carcinoembryonic antigen antibody labeled with ^{99m}Tc: the role of metabolism and kinetics. *Cancer Res* 1995;55:5777s–5785s.
15. Wessels BW, Rogus RD. Radionuclide selection and model absorbed dose calculations for radiolabeled tumor associated antibodies. *Med Phys* 1984;11:638–645.
16. Yorke E, Beaumier P, Wessels B, Fritzberg A, Morgan AC. Optimal antibody-radionuclide combinations for clinical radioimmunotherapy: a predictive model based on mouse pharmacokinetics. *Nucl Med Biol* 1991;18:827–835.
17. Sands H, Jones PL, Shah SA, Palme D, Vessella R, Gallagher BM. Correlation of vascular permeability and blood flow with monoclonal antibody uptake by human clouser and renal cell xenografts. *Cancer Res* 1988;48:188–193.
18. Baxter LT, Zhu H, Butler WF, Jain RK. Physiologically based pharmacokinetic model for specific and non-specific monoclonal antibodies and fragments in normal tissues and human tumor xenografts in nude mice. *Cancer Res* 1994;54:1517–1528.
19. Baxter LT, Zhu H, Mackensen DG, Jain RK. Biodistribution of monoclonal antibodies: scale up from mouse to man using a physiologically based pharmacokinetic model. *Cancer Res* 1995;55:4611–4622.
20. Jain RK. Delivery of molecular medicine to solid tumors. *Science* 1996;271:1079–1080.
21. Dedrick R. Animal scale up. *J Pharmacokin Biopharm* 1973; 1:435–461.
22. Strand SE, Zanzonico P, Johnson T. Pharmacokinetic modeling. *Med Phys* 1993;20:515–527.

23. Bischoff KB, Dedrick RL, Zaharko DS, Longstreth JA. Methotrexate pharmacokinetic. *J Pharmacol Sci* 1971;60:1128–1133.
24. Gerlowski LE, Jain RK. Physiologically based pharmacokinetic modeling: principles and applications. *J Pharmacol Sci* 1983;72:1103–1123.
25. Watson EE, Stabin G, Siegel JA. MIRD formulation. *Med Phys* 1993; 20:511–514.
26. Leichner PK, Kwok CS. Tumor dosimetry in radioimmunotherapy: methods of calculation for beta particles. *Med Phys* 1993;20:529–534.
27. Meredith RF, Johnson TK, Macey DJ, et al. Dosimetry of solid tumors. *Med Phys* 1993;20:583–592.
28. Bradwell AR, Fairweather DS, Dykes PW, Keeling A, Vaughan A, Taylor J. Limiting factors in the localization of tumors with radiolabeled antibodies. *Immunol Today* 1985;6:163–170.
29. Bradwell AR, Dykes P, Thomas G. Antibody targeting: theoretical considerations. In: Goldenberg DM, ed. *Cancer imaging with radiolabeled antibodies*. New York, NY: Kluwer Academic Publishers; 1990:11–25.
30. Rockoff SD, Goodenough D, McIntire KR. Theoretical limitations in the immunodiagnostic imaging of cancer with computed tomography and nuclear scanning. *Cancer Res* 1980;40:3054–3058.
31. Roberson PL, Buchsbaum DJ. Reconciliation of tumor dose response to external beam radiotherapy versus radioimmunotherapy with ^{131}I-labeled antibody for a colon cancer model. *Cancer Res* 1995;55:5811s–5816s.
32. Langmuir VK, Fowler JF, Knox SJ, Wessels BW, Sutherland RM, Wong JYC. Radiobiology of radiolabeled antibody therapy as applied to tumor dosimetry. *Med Phys* 1993;20:601–610.
33. Phillips T. Principles of radiobiology and radiation therapy. In: Carter S, Glatstein E, Livingston R, eds. *Principles of cancer treatment*. New York, NY: McGraw-Hill; 1985:58–87.
34. Sands H, Gallagher BM. Physiological, pharmacological and immunological aspects of antibody targeting. In: Zalutsky MR, ed. *Antibodies in radiodiagnosis and therapy*. Boca Raton, FL: CRC Press; 1989:129–151.
35. Schlom J, Hand PH, Greiner JW, et al. Innovations that influence the pharmacology of monoclonal antibody guided tumor targeting. *Cancer Res* 1990;50:820s–827s.
36. Buchsbaum DJ. Experimental approaches to increase radiolabeled antibody localization in tumors. *Cancer Res* 1995;55:5729s–5732s.
37. Knox SJ. Overview of studies on experimental radioimmunotherapy. *Cancer Res* 1995;55:5832s–5836s.
38. Carrasquillo JA, Sugarbaker P, Colcher D. Radioimmunoscintigraph of colon cancer with iodine-131-labeled B72.3 monoclonal antibody. *J Nucl Med* 1988;29:1022–1030.
39. Khaw B, Strauss HW, Narula J. "Magic bullets:" from muskets to smart bombs! *J Nucl Med* 1993;34:2264–2268.
40. Doerr RJ, Abdel-Nabi H, Krag D. Radiolabeled antibody imaging in the management of colorectal cancer. *Ann Surg* 1991;214:118–124.
41. Hellman S. Principles of radiation therapy. In: Rosenberg SA, Hellman S, De Vito V, eds. *Cancer*, vol. 1. Philadelphia, PA: J.B. Lippincott; 1992:2490.
42. Eger RR, Covell DG, Carrasquillo JA, et al. Kinetic model for the biodistribution of an ^{111}In-labeled monoclonal antibody in humans. *Cancer Res* 1987;47:3328–3336.
43. Thomas GD, Chappell MJ, Dykes PW. Effect of dose, molecular size, affinity and protein binding on tumor uptake of antibody or ligand: a biomathematical model. *Cancer Res* 1989;49:3290–3296.
44. Sung C, Shockley TR, Morrison PF, Dvorak HF, Yarmush ML, Dedrick RL. Predicted and observed effects of antibody affinity and antigen density on monoclonal antibody uptake in solid tumors. *Cancer Res* 1992;52:377–384.
45. Fujimori K, Covell DG, Fletcher JE, Weinstein JN. Modeling analysis of the global and microscopic distribution of immunoglobulin G, F(ab')$_2$ and Fab in tumors. *Cancer Res* 1989;49:5656–5663.
46. Fujimori K, Covell DG, Fletcher JE, Weinstein JN. A modeling analysis of monoclonal antibody percolation through tumors: a binding-site barrier. *J Nucl Med* 1990;31:1191–1198.
47. Fujimori K, Fisher DR, Weinstein JN. Integrated microscopic-macroscopic pharmacology of monoclonal antibody radioconjugates: the radiation dose distribution. *Cancer Res* 1991;51:4821–4827.
48. Weinstein JN, Eger RR, Covell DG. The pharmacology of monoclonal antibodies. *Ann NY Acad Sci* 1987;507:199–210.
49. Weinstein JN, van Osdol W. Early intervention in cancer using monoclonal antibodies and other biological ligands: micropharmacology and the "binding-site barrier." *Cancer Res* 1992;52:2747s–2751s.
50. Jain RK. Delivery of novel therapeutic agents in tumors: physiological barriers and strategies. *J Natl Cancer Inst* 1989;81:570–576.
51. Hindmarsh AC. LSODE and LSODI: two new initial value ordinary differential equation solvers. *ACM Signum Newsletter* 1980;15:10–11.
52. Rippe B, Haraldsson B. Transport of macromolecules across microvascular walls: the two-pore theory. *Phys Rev* 1994;74:163–219.
53. Baxter LT, Jain RK. Transport of fluid and macromolecules in tumors. III. Role of binding and metabolism. *Microvasc Res* 1990;41:5–23.
54. Jain RK. Determinants of tumor blood flow: a review. *Cancer Res* 1988;48:2641–2658.
55. Jain RK. Transport of molecules in the tumor interstitium: a review. *Cancer Res* 1987;47:3039–3051.
56. Wahl RL, Parker CW, Philpott GW. Improved radioimaging and tumor localization with monoclonal F(ab')$_2$. *J Nucl Med* 1983;24:316–325.
57. Colapinto EV, Humphrey PA, Zalutsky MR, et al. Comparative localization of murine monoclonal antibody Me1-14 F(ab')$_2$ fragment and whole IgG2a in human glioma xenografts. *Cancer Res* 1988;48:5701–5707.
58. Buchegger F, Pelegrin A, Delaloye B, Bischof-Delaloye A, Mach J-P. Iodine-131-labeled Mab F(ab')$_2$ fragments are more efficient and less toxic than intact anti-CEA antibodies in radioimmunotherapy of large human colon carcinoma grafted in nude mice. *J Nucl Med* 1990;31:1035–1044.